Lab on a Chip

COMMUNICATION

View Article Online
View Journal | View Issue

Cite this: *Lab Chip*, 2025, **25**, 4588

Received 20th February 2025,
Accepted 13th August 2025

DOI: 10.1039/d5lc00175g

rsc.li/loc

Inverse micelle mediated calcium chloride transportation for facile alginate gelation in microdroplets

Fuyang Qu,†*[a] Luoquan Li,†[a] Qinru Xiao[a] and Yi-Ping Ho *[abcde]

Block copolymer fluorosurfactants are frequently utilized to stabilize water–oil interfaces in droplet microfluidics, enabling parallel and compartmentalized biochemical reactions within individual droplets. Surfactants are able to self-assemble into inverse micelles with the concentration exceeding the critical micelle concentration (CMC), which has been identified as the main reason causing cross-contamination among droplets. This study explored the possibility to utilize the inverse micelles for passive cargo delivery from the fluorocarbon oil phase into the aqueous droplet interior, which has rarely been studied previously. We presented a novel strategy to load the molecular cargo, in this case calcium, into the inverse micelles and subsequently transport it into the water-in-oil droplets. Specifically, calcium chloride was firstly solvated with methanol and well-dispersed in fluorocarbon oil containing fluorosurfactants. Upon interaction with droplets containing un-crosslinked alginate stabilized by the same kind of fluorosurfactant, calcium ions were able to transport from inverse micelles through the water–oil interface and ultimately to the aqueous droplets, as observed by the successful production of alginate beads through ionic crosslinking of alginate in the microdroplets. The cytotoxicity of methanol was also validated to be minimal in two tested cell lines, suggesting the potential for broad adoption of alginate microbeads produced by the proposed approach.

[a] *Department of Biomedical Engineering, Faculty of Engineering, The Chinese University of Hong Kong, Hong Kong SAR, China. E-mail: qufy@link.cuhk.edu.hk, ypho@cuhk.edu.hk*
[b] *State Key Laboratory of Marine Pollution, City University of Hong Kong, Hong Kong SAR, China*
[c] *Hong Kong Branch of CAS Center for Excellence in Animal Evolution and Genetics, The Chinese University of Hong Kong, Hong Kong SAR, China*
[d] *The Ministry of Education Key Laboratory of Regeneration Medicine, Shatin, New Territories, Hong Kong SAR, China*
[e] *Centre for Novel Biomaterials, The Chinese University of Hong Kong, Shatin, New Territories, Hong Kong SAR, China*
† These authors contributed equally to this work.

1. Introduction

Water-in-oil (W/O) droplet microfluidics has emerged as a transformative and versatile tool in biological and chemical applications, for instance, droplet digital polymerase chain reaction (ddPCR),[1,2] protein crystallization,[3–5] single-cell analysis,[6–10] directed enzyme evolution,[11–13] and drug screening.[14,15] W/O droplets with a volume ranging from picoliters to nanoliters are produced uniformly at a high throughput (~kHz), allowing encapsulation of single mammalian cells, plant nuclei, bacteria, viruses, and/or molecular components for parallel analysis. Fluorocarbon oils are frequently utilized as the continuous phase due to their documented biocompatibility, high gas permeability, and chemical inertness.[16,17] To maintain compartmentalization from droplet coalescence, block copolymer surfactants with fluorous tail and hydrophilic head are commonly employed to stabilize the interface between fluorocarbon oil and aqueous phase by reducing surface tension and the thermodynamic driving force toward droplet fusion.[16–19] However, an addition of components into individual droplets may be required for many complex reactions including steps of reaction initiation, termination, or modification, where the barrier of surfactant needs to be transiently overcome. For example, a surfactant-stabilized droplet containing molecular barcodes is often fused with a droplet containing pre-amplified genomes from single cells, allowing barcoding the genomes extracted from a single cell.[8,9]

With surfactants present at the W/O interfaces, approaches categorized as active and passive methodologies are developed to allow additions of reagents into droplets. In the active approaches, external energy sources including electric fields,[20–24] thermal energies,[25] and surface acoustic waves (SAW)[26,27] are typically required. Electric fields are often applied across microchannels using integrated electrodes made of indium solder[20,21] or salt water,[22,23]

facilitating droplet electro-coalescence or pico-injection. In electro-coalescence, dipoles are induced when adjacent droplets containing high-conductivity solutions traverse an electric field region, resulting in coalescence due to the strong attractive Coulomb force.[28] Typically, the voltage is set to several hundreds of volts at frequencies of dozens of kHz to effectively induce droplet fusion. Similarly, reagents can be injected into individual droplets with controlled volume by fine-tuned droplet velocity and injection pressure in the presence of an electric field.[24] Another active approach involves destabilizing the interfaces of two proximate droplets using localized laser heating, potentially due to the evaporation of surfactants and the oil film between droplets.[25] For the SAW-based technique, the proposed mechanism entails the pushing and pulling of droplet pair interfaces by acoustic streaming in the oil phase, ultimately causing rupture and coalescence.[26,27] Despite their use in numerous chemical and biological assays, these active methods necessitate complex microfluidic devices embedded with electrodes, interdigital transducers, high-voltage modules, or lasers, requiring well-trained personnel for precise operation, thereby limiting their broader applications.

Passive methodologies, facilitating droplet coalescence without external energy input, represent relatively accessible means to deliver cargos into surfactant-stabilized droplets. Through the meticulous design of a flowing chamber within the microfluidic device, droplet coalescence has been observed when a pair of droplets is forcibly separated within the chamber, plausibly due to the formation of a nipple during droplet separation, leading to depletion of surfactants at the droplet interfaces.[29] Another example is demonstrated by reinjecting a collection of surfactant-stabilized droplets into a microfluidic device and controllably pair a surfactant-stabilized droplet with a droplet not fully covered by surfactants.[30,31] Experimental results have shown that the contact time of the pair of droplets and the surfactant coverage of un-stabilized droplets are critical for effective fusion.[31] Beyond passive droplet merging to deliver components into designated droplets, small molecules dissolved in the oil phase may also be gradually diffused into a collection of droplets. For instance, oxygen and carbon dioxide respiratory gases are permeable and soluble in fluorocarbon oils typically used in droplet microfluidics, thereby allowing gas supply to cells encapsulated in W/O droplets for investigation of an extended duration.[32]

Fundamentally, surfactants are essential for stabilizing W/O interfaces, producing the so-called inverse micelles when the surfactant concentration exceeds the critical micelle concentration (CMC). Inverse micelles formed by surfactants in fluorocarbon or hydrocarbon oils have been shown to facilitate transport of molecules, such as fluorophores, among W/O droplets or water-in-oil-in-water (W/O/W) double emulsions.[33–38] For instance, Y. Skhiri *et al.* have observed increased fluorophores dissolved in fluorous oil at surfactant concentrations above the CMC, because fluorophores incorporated into surfactant-assembled inverse micelles.[33] The fluorophore exchange rate between droplets also raises with the surfactant concentration, indicating that the inverse micelles may facilitate inter-droplet transport as

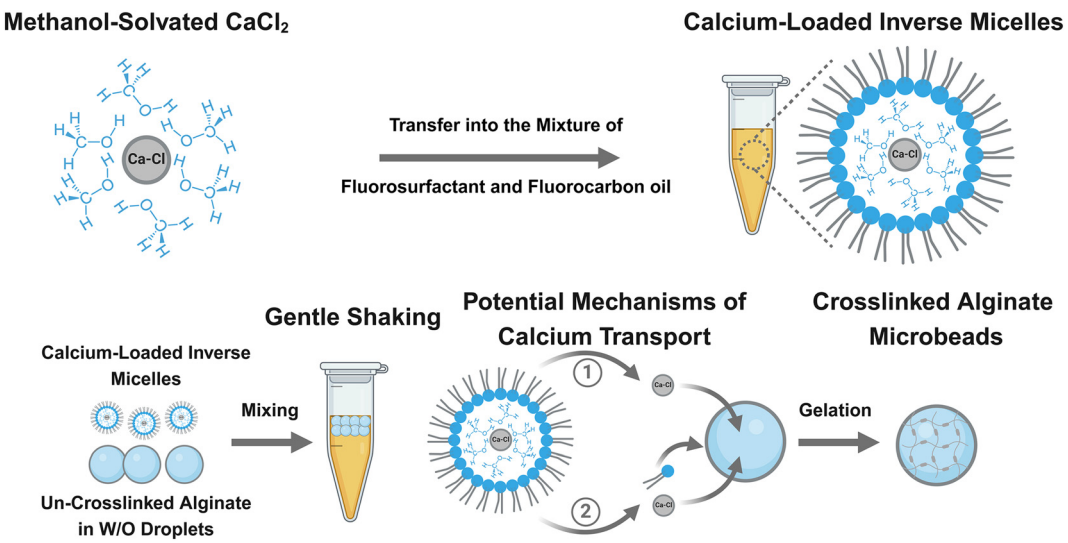

Fig. 1 Schematic of the inverse micelle mediated cargo transportation (IMCT). Calcium chloride ($CaCl_2$), as a model, is pre-dissolved in methanol and subsequently transferred into fluorocarbon oil supplemented with commercially available molecular fluorosurfactant, producing inverse micelles containing methanol-solvated $CaCl_2$. Subsequently, the same fluorosurfactant is used to stabilize droplets containing un-crosslinked alginate. Upon mixing of the methanol-solvated $CaCl_2$ containing inverse micelles and the alginate droplets, alginate within the droplets is observed to be crosslinked. Gelation of alginate is plausibly through: (1) calcium ion diffusion and partition from the inverse micelle through the fluorocarbon oil and subsequently to the aqueous droplet interior; and (2) competition of fluorosurfactant from the methanol-solvated $CaCl_2$ containing inverse micelles and the Pluronic F-127 surfactant on the interfaces of W/O droplets, resulting in dismantling of inverse micelles, and consequently allowing the released calcium ions to be transported into the water-in-oil droplets. Fig. 1 is created with **https://BioRender.com**.

nanocontainers. On the other hand, at the surfactant concentration below CMC, leakage of fluorescent dye across the W/O/W double emulsions decreases, further suggesting the important role of inverse micelles in molecular transport.[34] In a separate study, the size of diffusing entities aligns with the dimension of inverse micelles based on a calculation from the diffusion coefficients, corroborating the role of inverse micelles as mediators of small organic molecules transporting across droplets.[35]

Inspired by these findings, this study explores the possibility to use molecular cargo-loaded inverse micelles as a facile approach for passive cargo transportation into surfactant-stabilized droplets, termed inverse micelle mediated cargo transportation (IMCT). As a proof-of-concept, calcium chloride ($CaCl_2$) is selected as a cargo to-be-delivered into fluorosurfactant stabilized W/O droplets. As illustrated in Fig. 1, $CaCl_2$ is dissolved in methanol, forming a methanol-solvated structure, in which the calcium and chloride ions interact with methanol molecules through element pairs, including Ca–O, Cl–O, and Ca–C.[39,40] At the $CaCl_2$ concentration of around 3.6 M in methanol, a hypothetical solvate structure model assumes that each Ca–Cl ion pair is surrounded by six methanol molecules, based on previously presented X-ray diffraction studies.[39] When the calcium-containing methanol solution is introduced to a mixture of fluorocarbon oil and fluorosurfactant, such as the commercially available Pico-Surf, inverse micelles, depicted as discrete nanostructures composed of a water core surrounded by fluorosurfactant, encapsulating the methanol-solvated $CaCl_2$, as shown in Fig. 1, are produced. The Pico-Surf fluorosurfactant is composed of Jeffamine-$PFPE_2$ (ref. 18) and the hydrophilic head with amide, methylene, and methyl groups is assumed to interact with methanol by hydrogen bonding and hydrophobic interactions, thus enabling the stabilization of calcium-loaded inverse micelles. Mixing the cargo-loaded inverse micelles with un-crosslinked alginate droplets, stabilized with the same type of fluorosurfactant, is able to initiate an immediate transportation of calcium ions from the inverse micelles to the aqueous core of W/O droplets *via* two potential mechanisms (Fig. 1), subsequently promoting alginate gelation in a facile manner. Alginate, as one of the natural biomaterials, has been demonstrated for a wide range of biomedical applications including drug delivery,[41–43] tissue engineering,[44,45] and 3D cell culture.[46–49] Chemically, alginate consisting of β-D-mannuronic and α-L-guluronate residues can be crosslinked readily in the presence of divalent cations, with calcium ions being the most commonly used to form physical networks.[41] To produce alginate microbeads, droplet microfluidic methods are widely employed,[50] in systems containing either hydrocarbon oils (*e.g.*, vegetable oil, hexadecane, and mineral oil)[51–58] or fluorocarbon oils (*e.g.*, HFE7500 and FC40).[59–61] Given their gas permeability and biocompatibility, fluorocarbon oils have become increasing attractive for droplet-based biological applications.[16,17] When it comes to the preparation of alginate microbeads by the fluorocarbon oil system, gelation of the W/O droplets containing un-crosslinked alginate solution and Ca-EDTA requires an addition of acetic acid to the oil phase.[59] However, the acidic pH, below the physiological range, is shown harmful to cells. This issue has been largely addressed by introducing competitive ligands, the competitive ligand exchange crosslinking (CLEX) method, which maintained cell viability by keeping the pH at 6.7 during the gel bead preparation.[60] Notably, alginate gelation is shown to be swift under a pH below 6.7, however, clogging in the microfluidic channel may consequently occur. Under a pH above 7.2, on the other hand, gelation is observed to be insufficient, resulting in inadequate calcium ions for alginate gelation. Therefore, precise pH control within a narrow range is essential, complicating the preparation procedures. Additionally, chelators such as EDTA and EDDA in the gelation system may also react with other metal ions, potentially affecting enzyme activity in cells.[61] A chelate-free approach has been subsequently proposed, where calcium ions are introduced to the alginate-containing droplets *via* picoinjection.[61] However, the reported method involved a complex chip design with embedded metal electrodes, and the operation of injection may not be favorable for untrained personnel. In this report, the proposed schematic of IMCT provides a facile approach for the controlled transportation of calcium ions into the droplet interior for alginate gelation with fluorocarbon oil as the continuous phase. Given the mild concentration and short exposure of methanol in the proposed process, cell viability has also been observed to be minimally altered. Taken together, the proposed scheme represents a biocompatible, facile, and user-friendly strategy to transport molecular cargos from fluorocarbon oil to fluorosurfactant stabilized W/O droplets, which is expected to expand the tool sets for droplet-microfluidics based biochemical applications.

2. Materials and methods

Materials and chemicals

5% (w/w) Pico-Surf™ dissolved in NOVEC™ 7500 fluorocarbon oil, hereafter abbreviated as Pico-Surf, was acquired from Sphere Fluidics (UK). Droplet generation oil with surfactant (Catalog No.: 1863005) was from Bio-Rad (USA). Methanol, $CaCl_2$, 1*H*,1*H*,2*H*,2*H*-perfluoro-1-octanol (PFO), alginate (Catalog No.: A2033), Pluronic F-127 (Catalog No.: P2433), Tween 20 (P1379), and DMSO were purchased from Sigma Aldrich (USA). Polydimethylsiloxane (PDMS) base and curing agent were from Dow Corning (USA). SU8-3050 photoresist and developer were purchased from Kayaku Advanced Materials (USA) and MicroChem (USA), respectively. Dulbecco's modified Eagle medium (DMEM), FBS, and

penicillin–streptomycin were acquired from Gibco (USA). MTT (3-(4,5-dimethylthiazol-2-yl)-2,5-diphenyltetrazolium bromide) (Catalog No.: M6494) was purchased from Thermo Fisher Scientific (USA).

Characterization by dynamic light scattering

The inverse micelle size distributions from three distinct samples were analyzed by dynamic light scattering (DLS, DelsaMax Pro, Beckman Coulter, USA). Sample A comprised 500 μL of NOVEC™ 7500 fluorocarbon oil with 5% (w/w) Pico-Surf. Sample B was prepared by mixing 5 μL of methanol with 500 μL of the same fluorocarbon oil containing 5% (w/w) Pico-Surf, followed by vortexing for approximately 2 minutes, achieving a final methanol concentration of 1% (v/v). For sample C, 5 μL of methanol containing 1.8 M $CaCl_2$ was dispersed into 500 μL of the fluorocarbon oil with 5% (w/w) Pico-Surf through vortexing for about 2 minutes, resulting in a final concentration of 1% (v/v) methanol and 18 mM calcium chloride. Each sample was measured at least three times *via* DLS at 25 °C, with the viscosity and dielectric constant values set at 1.24 cP and 5.8, respectively.

Elemental analysis of sediments

5 μL of methanol containing 3.6 M $CaCl_2$ was firstly dispersed into 500 μL of fluorocarbon oil with 5% (w/w) Pico-Surf through vortexing for approximately 2 minutes. The solution became turbid after incubating for about 10 minutes, and sediments were identified by centrifugation at 1000*g* for 5 minutes. These sediments were then washed three times with 500 μL NOVEC™ 7500 fluorocarbon oil and resuspended in 500 μL fluorocarbon oil. The elemental composition of the sediments was analyzed using scanning electron microscopy-energy dispersive spectroscopy (SEM-EDS, Quanta 400F, FEI, USA). Approximately 10 μL of fluorocarbon oil containing sediments was dropped onto double-sided carbon tape. After drying for about 10 minutes at room temperature, the sample was coated with platinum to prevent charge accumulation. EDS data was collected from three different points on the sample surface at an accelerating voltage of 20 kV.

Fabrication of microfluidic chips

The microfluidic chip was fabricated by the widely adopted soft photolithography. Briefly, the chip pattern (Fig. S1) was designed using CAD software (Autodesk, San Rafael, USA) and subsequently printed on a transparency film with a resolution of 25 400 DPI (MicroCAD Photo-Mask Ltd., Shenzhen, China). Following the manufacturer's instructions, SU8-3050 photoresist (Kayaku Advanced Materials, USA) was coated onto a 4-inch silicon wafer. Through appropriate UV exposure and development, the un-crosslinked SU8-3050 photoresist was removed using the SU8 developer (MicroChem, USA). After post-exposure bake, the fabricated SU8 master mold was measured to be approximately 45 μm in height.

Polydimethylsiloxane (PDMS) base and curing agent (Dow Corning, USA) were thoroughly mixed in a weight ratio of 10 : 1 and poured onto the fabricated master mold. After degassing to eliminate bubbles, the PDMS mixture was fully cured in an oven at 80 °C overnight. Subsequently, the crosslinked PDMS was peeled from the mold and cut into slabs. The inlets and outlets were generated using a puncher with a 1.0 mm diameter (Integra LifeSciences, USA). Finally, the PDMS slabs were bonded to a cover glass pre-coated with a thin layer of semi-cured PDMS (base and curing agent in a weight ratio of 2 : 1). The assembled microfluidic chips were further incubated in an oven at 80 °C overnight to strengthen the bonding.

IMCT-based alginate gelation

An alginate solution, as the aqueous phase, was prepared in a concentration of 1% (w/v) alginate and 0.1% (w/v) Pluronic F-127 or 0.1% (v/v) Tween 20 in PBS. The oil phase containing 0.5% (w/w) Pico-Surf surfactant in NOVEC™ 7500 fluorocarbon oil was also prepared. The aqueous and oil phases were separately loaded into two 1 mL syringes (BD Biosciences, USA), which were connected to the two inlets on the microfluidic chip (Fig. S1) using 23G needles (BD Biosciences, USA) and PFPE tubing (Cole-Parmer, USA). Controlled by two syringe pumps (PHD ULTRA, Harvard Apparatus, USA), the alginate solution was emulsified by the oil phase to produce microdroplets, with volumetric flow rates set at 2.5 μL min^{-1} and 10 μL min^{-1}, respectively.

Further, fluorocarbon oil dispersed with $CaCl_2$ was prepared by adding varying amounts of methanol (0.125 μL, 0.25 μL, 0.5 μL, and 1 μL) containing 3.6 M $CaCl_2$ to 300 μL of fluorocarbon oil with 5% (w/w) Pico-Surf surfactant, resulting in final $CaCl_2$ concentrations in the oil of 1.5 mM, 3 mM, 6 mM, and 12 mM, respectively. Subsequently, alginate gelation was assessed by adding 30 μL droplets containing 1% (w/v) un-crosslinked alginate and 0.1% (w/v) Pluronic F-127 or 0.1% (v/v) Tween 20 into the 300 μL oil phase dispersed with calcium chloride. After shaking and incubating for one to twenty minutes, the alginate microbeads were released by adding 20 μL of 1*H*,1*H*,2*H*,2*H*-perfluoro-1-octanol (PFO) to destabilize the water–oil interfaces. Bright-field images of the alginate microbeads were captured using an inverted microscope (ECLIPSE Ti-U, Nikon, Japan).

Droplets containing un-crosslinked alginate and 1% (w/v) Pluronic F-127 were also prepared using the fluorocarbon oil containing 0.1× Bio-Rad surfactant with volumetric flow rates of 10 μL min^{-1} for the oil and 2.5 μL min^{-1} for the aqueous phase. Further, 0.5 μL of methanol containing 3.6 M $CaCl_2$ was dispersed into 300 μL oil phase with undiluted Bio-Rad surfactant by sonication for 2 minutes. Finally, 30 μL droplets were introduced into the 300 μL oil with $CaCl_2$ to prepare

alginate microbeads through one minute of shaking incubation.

Characterization of alginate beads

The circularity of alginate beads was quantified by using eqn (1):

$$\text{Circularity} = \frac{4\pi A}{P^2} \quad (1)$$

A and P are the projection area and perimeter, respectively, measured by ImageJ (NIH, USA).

The mechanical stiffness of produced alginate beads was evaluated by an optical fiber-based interferometry nanoindenter (Pavone, Optics11 Life). Indentation measurements were conducted on at least three alginate beads with an indenter having a spherical tip radius of 3 μm and a stiffness of 0.018 N m^{-1}. The measured forces were processed by hydrodynamic correction.[62] The Young's modulus of alginate beads was extracted by fitting the force–indentation curve with a double contact model (derived from the Hertz model and the Johnson–Kendall–Roberts (JKR) model),[63] according to eqn (2), where the factor k was calculated based on eqn (3)–(5):

$$F = \frac{4}{3}\frac{ER_{12}^{1/2}}{1-\nu^2}(kd)^{3/2} \quad (2)$$

$$k = \frac{R_{32}^{1/3}}{R_{12}^{1/3} + R_{32}^{1/3}} \quad (3)$$

$$\frac{1}{R_{12}} = \frac{1}{R_1} + \frac{1}{R_2} \quad (4)$$

$$\frac{1}{R_{32}} = \frac{1}{R_2} + \frac{1}{R_3} \quad (5)$$

F, R_1 (3 μm), R_2 (33.9 μm), R_3 (∞), E, ν (0.5), and d are the indentation force, radius of the indenter, radius of alginate beads, radius of the substrate, Young's modulus, Poisson's ratio, and indentation depth, respectively.

Cell culture

HEK293 cells (ATCC Catalog No.: CRL-1573) and A549 cells (ATCC Catalog No.: CCL-85) were cultured in cell culture dishes (SPL, Korea) at 37 °C with 5% CO_2. The culture medium consisted of Dulbecco's modified Eagle medium (DMEM, Gibco, USA) supplemented with 10% FBS (Gibco, USA) and 1% penicillin–streptomycin (Gibco, USA), and was replaced every two days to ensure optimal cell culture conditions. Cells were harvested by treating with trypsin for 5 minutes when cell confluence reached 70–90%, in preparation for the subsequent MTT assay.

MTT cell viability assay

The cytotoxicity of methanol was assessed using the MTT assay. Specifically, 20 000 HEK293 or A549 cells per well were seeded into two distinct 96-well plates (SPL, Korea). After overnight incubation at 37 °C with 5% CO_2, the cells were treated with a culture medium containing 2% (v/v) or 4% (v/v) methanol for one minute. Subsequently, a 0.5 mg mL^{-1} MTT solution was added and incubated with the cells for four hours at 37 °C. Finally, the MTT solution was removed, and the formazan product within the cells was solubilized by adding 100 μL of DMSO (Sigma-Aldrich, USA) in each well. The optical absorbance was then measured at 540 nm using a microplate reader (SpectraMax M3, Molecular Devices, USA).

3. Results and discussion

To substantiate the proposition that $CaCl_2$, in conjunction with methanol, was encapsulated within inverse micelles assembled by the fluorosurfactant, we conducted a dimensional analysis of the inverse micelles utilizing dynamic light scattering (DLS). As illustrated in Fig. 2a and d, the inverse micelles in the fluorocarbon oil (NOVEC™ 7500) containing 5% (w/w) Pico-Surf surfactant exhibited a diameter of 11.1 ± 0.2 nm. Upon the introduction of 1% (v/v) methanol into the oil of identical surfactant concentration, the average hydrodynamic diameter of the inverse micelles augmented by approximately 11.7%, reaching a diameter of 12.4 ± 0.2 nm (Fig. 2b and d). This increase in size was plausibly attributed to the inclusion of methanol molecules within the inverse micelles, facilitated by the extant non-covalent interactions between the hydrophilic segment of the surfactant and the methanol molecules. Moreover, the size of inverse micelles expanded to approximately 16.3 ± 1.0 nm (Fig. 2c and d), when methanol-solvated $CaCl_2$ was introduced into the oil–fluorosurfactant mixture at final concentrations of 1% (v/v) and 18 mM for methanol and $CaCl_2$, respectively. The further increase of the inverse micelle size in the presence of methanol-solvated $CaCl_2$ corroborated with the hypothesis that the produced inverse micelles were co-loaded with $CaCl_2$ and methanol molecules. It is noteworthy that the Pico-Surf surfactant might also assemble into larger vesicles of hydrodynamic diameters of around 100–200 nm, as shown in Fig. 2a. Upon the introduction of 1% (v/v) methanol into the fluorocarbon oil, the main peak intensity of the vesicle population was observed below 10%, as depicted in Fig. 2b, indicating the potential competition of fluorosurfactants between the populations of inverse micelles and vesicles. Further obvious disintegration of vesicular structures is seen in Fig. 2c, where the population of vesicles was almost suppressed, suggesting that the fluorosurfactants were significantly competed out for the structural preference of inverse micelles in the co-presence of methanol molecules and $CaCl_2$.

It was observed that the mixture of methanol-solvated $CaCl_2$ containing fluorocarbon oil turned visually turbid after a certain period. For example, in the sample containing 1% (v/v) methanol and 36 mM $CaCl_2$, the clear solution became turbid within 10 minutes, as shown in Fig. 3a, presumably

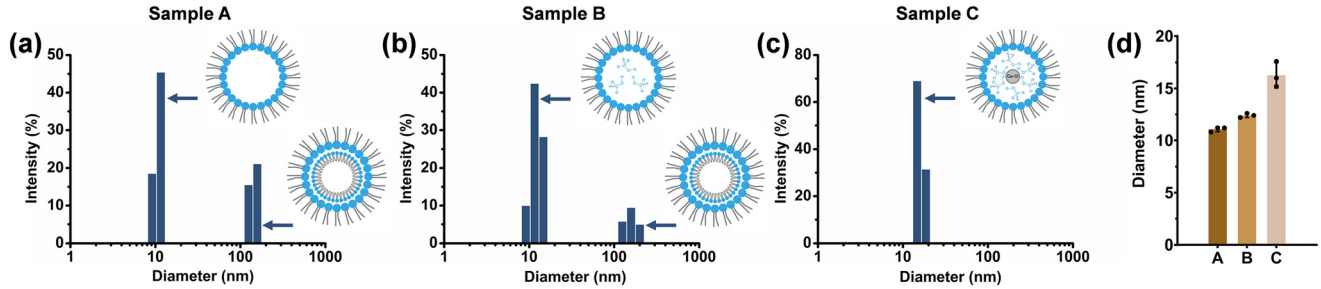

Fig. 2 Hydrodynamic diameters characterized by dynamic light scattering. (a) Size distribution profile of sample A, *i.e.* 5% (w/w) Pico-Surf dissolved in fluorocarbon oil, serves as the control, (b) sample B, and (c) sample C supplemented with 1% (v/v) of methanol and methanol-solvated $CaCl_2$ (1% (v/v) of methanol and 36 mM $CaCl_2$), respectively, in identical concentration of Pico-Surf-containing fluorocarbon oil. The populations of inverse micelles and vesicles were observed in both (a) and (b), whereas the population of vesicles was relatively obscure in (c). (d) The averaged hydrodynamic diameters of inverse micelles measured from the three samples. Data presented as the mean ± SD. This figure is partially created with **https://BioRender.com**.

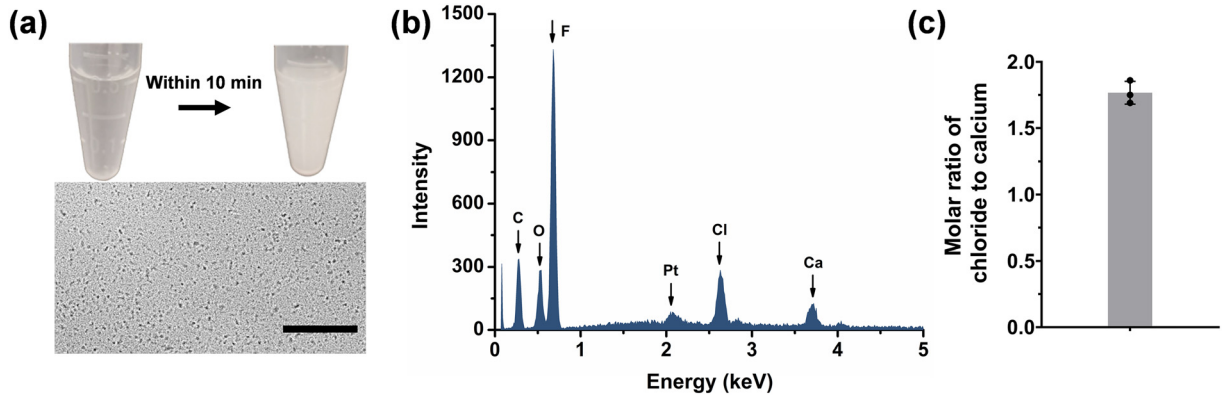

Fig. 3 (a) The as-prepared methanol-solvated $CaCl_2$ (1% (v/v) methanol, 36 mM $CaCl_2$) containing fluorocarbon oil was observed visually to be turbid after around 10 minutes of incubation at room temperature. A typical bright-field image showing the sediments in the turbid solution. Scale bar: 50 μm. (b) EDS analysis of the collected sediments. (c) Molar ratio of chloride to calcium calculated from the peaked intensity of EDS measurement. Data presented as the mean ± SD.

due to the thermal instability of $CaCl_2$ loaded inverse micelles. To examine this postulation, the turbid solution was centrifuged and the collected sediments were characterized *via* energy dispersive spectroscopy (EDS). As shown in Fig. 3b, the spectroscopic peaks of chloride and calcium elements were identified and the molar ratio of Cl and Ca calculated from the intensity peak was around 1.8 (Fig. 3c), closely resembling the stoichiometric ratio characteristic of $CaCl_2$, *i.e.* 2, suggesting that the calcium and chloride ions released from the inverse micelles may form $CaCl_2$, reaching the global energy minimum thereof, and precipitate in the oil phase. Note that the spectroscopic peaks of carbon, oxygen, and fluorine indicated the presence of residual fluorocarbon oil in the sediments, whereas the detected platinum was attributed to the metal coating for preventing electric charge accumulation on insulating samples.

Taking advantages of the instability of methanol-solvated $CaCl_2$ encapsulated inverse micelles, we subsequently explored whether the $CaCl_2$-loaded inverse micelles may serve as a carrier. As a proof-of-concept, transport of released $CaCl_2$ into W/O droplets containing un-crosslinked alginate, stabilized by identical fluorosurfactants, was examined by gelation of alginate initiated by divalent ions, *i.e.* Ca^{2+}. To avoid confounding interference of turbidity during experiments, the supplemented $CaCl_2$ and methanol concentrations were first optimized at 12 mM and 0.33% (v/v), respectively. In this scenario, the methanol-solvated $CaCl_2$ containing fluorocarbon oil was observed visually to be clear for at least 30 minutes (data not shown), allowing sufficient handling time. On the other hand, monodisperse Pico-Surf surfactant stabilized W/O droplets (44.5 ± 2.0 μm, Fig. 4a) containing un-crosslinked 1% (w/v) alginate in PBS were produced by a flow-focusing based droplet generator (Fig. S1). 30 μL of these droplets were mixed with 300 μL of methanol-solvated $CaCl_2$ containing fluorocarbon oil followed by approximately one minute of gentle shaking. Upon an addition of the droplet breaking agent (1*H*,1*H*,2*H*,2*H*-perfluoro-1-octanol, PFO), crosslinked alginate microbeads were observed to be expanded as shown in Fig. 4b with the diameter measured at 67.7 ± 5.0 μm (Fig. 4c), due to the swelling of beads in pure water, similar to the observations in previous studies.[64,65] Swelling of beads

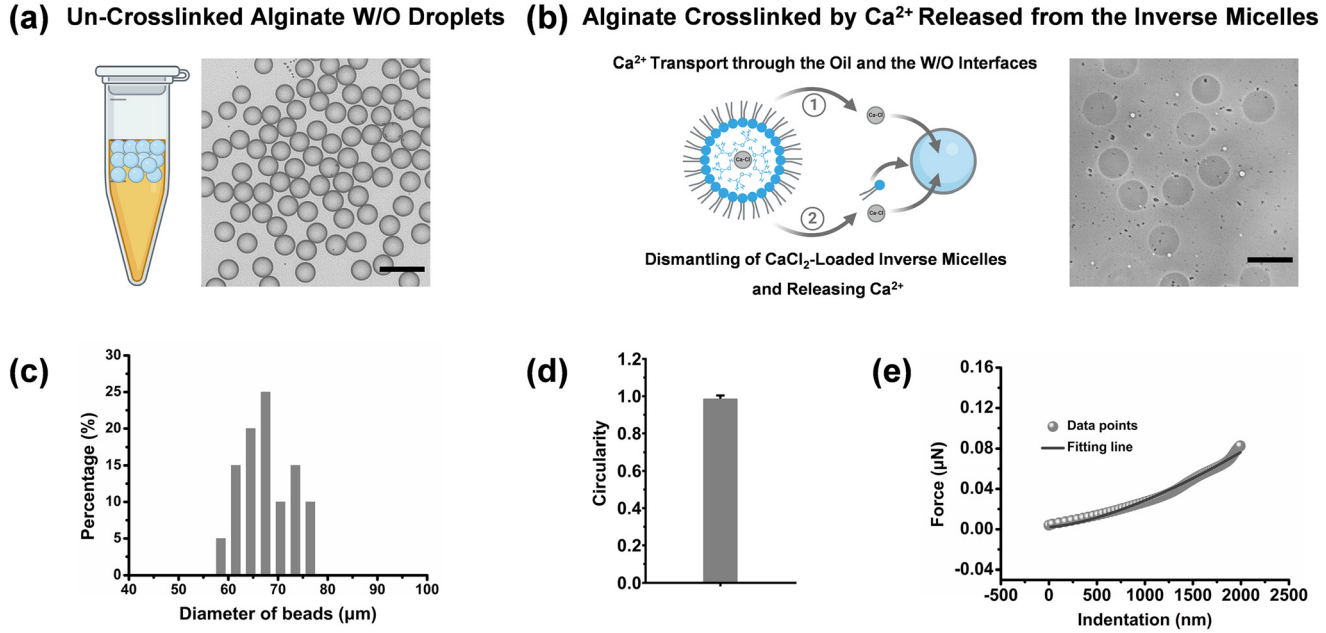

Fig. 4 IMCT-based alginate gelation. (a) A representative bright-field image showing the un-crosslinked alginate (1% w/v) encapsulated in W/O droplets stabilized by 0.5% (w/w) Pico-Surf in fluorocarbon oil. (b) Mixing the $CaCl_2$-loaded inverse micelles (calcium concentration in the oil phase: 12 mM) with the un-crosslinked alginate W/O droplets, followed by one minute shaking incubation to allow calcium transportation into droplets by two possible mechanisms. Crosslinked alginate beads were visually observed under a bright-field microscope, through which the size and circularity were characterized as shown in (c) and (d), respectively (n = 20). (e) A representative force–indentation plot measured from the as-prepared alginate beads. Scale bar: 100 μm.

was minimized by releasing the beads in PBS buffer containing 50 mM $CaCl_2$, as conducted in ref. 51, and the resulting bead size was measured to be 28.2 ± 1.7 μm (Fig. S2). Nevertheless, alginate beads produced in Fig. 4c showed decent circularity (~0.986) as shown in Fig. 4d, showcasing the facile transport of $CaCl_2$ through the proposed IMCT method, henceforth producing well-crosslinked alginate beads. Furthermore, the stiffness of the as-prepared alginate beads was characterized by a nanoindenter as shown by a representative force–indentation curve in Fig. 4e. The estimated Young's modulus of 21.3 ± 4.8 kPa was in the range of crosslinked alginate previously studied with similar alginate percentages,[66] demonstrating that the alginate beads produced by IMCT were at a comparable level of crosslinking.

Additionally, inclusion of Pluronic F-127, a hydrophilic nonionic surfactant yet cyto-compatible,[67,68] was observed to be essential to the IMCT-based gelation process. Without an addition of F-127, alginate gelation was incomplete even with optimizations by reducing the concentration of Pico-Surf to 0.1% (w/w) to minimize surfactant coverage on the W/O interfaces, or extending the shaking incubation to 20 minutes for further diffusion of calcium ions into the W/O droplets. Pluronic F-127 is often used to interface the water and oil phases and is anticipated to facilitate the transport of $CaCl_2$ from the oil phase to the aqueous phase of W/O droplets by two possible mechanisms as illustrated in Fig. 1 and 4b. The first potential mechanism involves the instability of $CaCl_2$-loaded inverse micelles as described previously. The calcium ions released from the inverse micelles are hypothesized to rapidly bind with Pluronic F-127 at the W/O interface through non-covalent interactions, such as Ca–O and Ca–C, and subsequently be transported into the aqueous phase given the dynamic characteristic of water–oil films. The other possibility is that the $CaCl_2$-loaded inverse micelles might disassemble due to the competition between Pico-Surf surfactant from inverse micelles and Pluronic F-127 molecules for stabilizing the W/O interfaces, thus bringing calcium ions in proximity to and subsequently allowing calcium ions to be transported into the droplet interior. Of note, polymeric micelle disassembly is also one of the major mechanisms allowing drug release given the interaction of polymeric micelles with cells or tissues.[69] Furthermore, the observation of Pluronic F-127 in promoting calcium delivery also corroborated with a previous simulation result, where the molecule transportation at the W/O interfaces was identified as the rate-limiting step.[70] However, the optimized structure of the hydrophilic surfactant warrants further study. As noted from Fig. S3, a counterpart replacing F-127 by 0.1% (v/v) of Tween 20 also mediated calcium transfer from the oil phase into the droplets, producing alginate beads, given that Tween 20 function similarly to F-127 anchoring at the oil–water interface. Yet, the produced beads were observed to be heterogeneous in size and in non-circular shape, possibly due to the shorter hydrophobic tail of Tween 20 than that of F-127.

Acknowledging that organic solvents, including methanol, may function as a strong dehydrant and cause

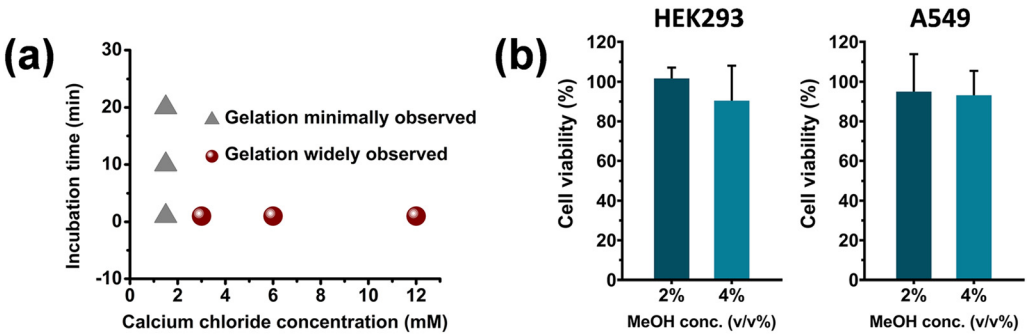

Fig. 5 Alginate microbead preparation and cytotoxicity of methanol. (a) Alginate gelation under varied incubation time and calcium chloride concentrations. (b) Cytotoxicity of methanol against two cell lines HEK293 and A549. Data presented as the mean ± SD.

precipitation of cellular proteins, we subsequently screen a range of methanol-solvated $CaCl_2$ concentrations for sufficient alginate gelation. Specifically, methanol-solvated $CaCl_2$ containing fluorocarbon oil was prepared with the final $CaCl_2$ concentrations of 1.5–12 mM, where the final methanol concentrations were 0.04–0.33% (v/v), respectively. Following similar procedures to the above-described, W/O droplets were broken by the droplet breaking agent and gelation of alginate was assessed by whether alginate beads were visually observed under bright-field imaging. As noted from Fig. 5a, alginate beads were widely observed with the $CaCl_2$ concentration of 3 mM and above, however, gelation was almost infeasible with the $CaCl_2$ concentration below 1.5 mM. Even with an extended incubation of up to 20 minutes, very few crosslinking beads were observed (Fig. S4). Assuming nearly complete transportation of calcium from the oil into the aqueous phase, the tested calcium concentrations were estimated 15 mM, 30 mM, 60 mM, and 120 mM in droplets based on the total volume of added droplets (*i.e.* 30 μL droplets were introduced in 300 μl oil phase containing 1.5 mM, 3 mM, 6 mM, and 12 mM $CaCl_2$, respectively). The observation of alginate gelation at $CaCl_2$ concentrations of 30 mM or above aligned with previous findings that alginate gelation was effectively achieved with the concentration of 25 mM $CaCl_2$ or above.[59] Additionally, alginate gelation within just one minute was proved sufficient, as evidenced by the minimal size variation between one- and five-minute incubation with 12 mM $CaCl_2$ in the oil phase (Fig. S5).

Subsequently, the methanol cytotoxicity was examined by the MTT assay. Corresponding to the validated $CaCl_2$ concentrations for effective alginate gelation shown in Fig. 5a, the methanol concentrations in the droplets were calculated to be 0.83% (v/v), 1.7% (v/v), and 3.3% (v/v), assuming complete methanol transport into the droplets during gelation. Herein, two cell lines, HEK293 and A549, were subjected to methanol treatment at concentrations of 2% (v/v) and 4% (v/v), both higher than the methanol concentrations introduced in the process, for one minute. As shown in Fig. 5b, cell viability (normalized to untreated cells) was close to 90% or higher, suggesting minimal alteration of cell viability for the presented IMCT-based alginate gelation.

In addition to Pico-Surf surfactant, the observed alginate gelation also holds valid for other PFPE-based fluorosurfactants. The commercially available Bio-Rad surfactant was also tested similarly to previously described. However, 2 minutes of sonication was observed necessary to effectively disperse methanol-solvated calcium chloride into the oil with the Bio-Rad surfactant, achieving a final concentration of $CaCl_2$ and methanol at 6 mM and 0.17% (v/v), respectively. The necessitation of sonication for dispersion might be attributed to the compositional differences between the Bio-Rad surfactant (PEG-$PFPE_2$) and the Pico-Surf surfactant (Jeffamine-$PFPE_2$). Moreover, these surfactants might also differ in their inverse packing parameters, which have been reported to influence the formation of inverse micelles.[34] Alginate microbeads were also prepared by incubating droplets containing 1% (w/v) alginate and 0.1% (w/v) Pluronic F-127 with the oil phase containing the Bio-Rad surfactant and 6 mM $CaCl_2$, using a one-minute shaking incubation (Fig. S6).

4. Conclusion

The potential of the IMCT-based strategy is witnessed by the facile production of alginate beads as presented in this study. The molecular cargos $CaCl_2$ is prepared in the form of methanol-solvated $CaCl_2$. Upon mixing of methanol-solvated $CaCl_2$ with fluorocarbon oil containing fluorosurfactant, such as Pico-Surf, inverse micelles encapsulating $CaCl_2$ are produced, as characterized by the increased diameter of inverse micelles through DLS. Crosslinking of alginate is achieved facilely by a brief incubation of these $CaCl_2$-loaded inverse micelles with W/O droplets containing un-crosslinked alginate. The cytotoxicity is proven subtle with the relatively low concentration and short exposure to methanol involved in the process. In conclusion, the inverse micelle-mediated cargo delivery presents an effective, undemanding, and biocompatible alternative against existing strategies for the production of alginate microbeads using microfluidics. Moreover, the operating mechanism is expected to open up new

possibilities for conducting complex biochemical reactions for microdroplet-based applications.

Conflicts of interest

The authors declare no conflict of interest.

Data availability

Supplementary information is available. See DOI: **https://doi.org/10.1039/D5LC00175G**.

The data supporting this article have been included as part of the SI.

Acknowledgements

This work was funded by the Research Grants Council of the Hong Kong Special Administrative Region, China (Project #: CUHK 14219922, 14207424 and C5005-23WF), the Marine Conservation Enhancement Fund (MCEF20108_L02), the Innovation and Technology Fund (ITS/217/21), and the VC Discretionary Fund provided by The Chinese University of Hong Kong (Project No. 8601014).

References

1 B. J. Hindson, K. D. Ness, D. A. Masquelier, P. Belgrader, N. J. Heredia, A. J. Makarewicz, I. J. Bright, M. Y. Lucero, A. L. Hiddessen, T. C. Legler, T. K. Kitano, M. R. Hodel, J. F. Petersen, P. W. Wyatt, E. R. Steenblock, P. H. Shah, L. J. Bousse, C. B. Troup, J. C. Mellen, D. K. Wittmann, N. G. Erndt, T. H. Cauley, R. T. Koehler, A. P. So, S. Dube, K. A. Rose, L. Montesclaros, S. Wang, D. P. Stumbo, S. P. Hodges, S. Romine, F. P. Milanovich, H. E. White, J. F. Regan, G. A. Karlin-Neumann, C. M. Hindson, S. Saxonov and B. W. Colston, *Anal. Chem.*, 2011, **83**, 8604–8610.

2 T. Suo, X. Liu, J. Feng, M. Guo, W. Hu, D. Guo, H. Ullah, Y. Yang, Q. Zhang, X. Wang, M. Sajid, Z. Huang, L. Deng, T. Chen, F. Liu, K. Xu, Y. Liu, Q. Zhang, Y. Liu, Y. Xiong, G. Chen, K. Lan and Y. Chen, *Emerging Microbes Infect.*, 2020, **9**, 1259–1268.

3 J. Ferreira, F. Castro, F. Rocha and S. Kuhn, *Chem. Eng. Sci.*, 2018, **19**, 232–244.

4 N. Pham, D. Radajewski, A. Round, M. Brennich, P. Pernot, B. Biscans, F. Bonneté and S. Teychené, *Anal. Chem.*, 2017, **89**, 2282–2287.

5 B. Zheng, L. S. Roach and R. F. Ismagilov, *J. Am. Chem. Soc.*, 2003, **125**, 11170–11171.

6 E. Z. Macosko, A. Basu, R. Satija, J. Nemesh, K. Shekhar, M. Goldman, I. Tirosh, A. R. Bialas, N. Kamitaki, E. M. Martersteck, J. J. Trombetta, D. A. Weitz, J. R. Sanes, A. K. Shalek, A. Regev and S. A. McCarroll, *Cell*, 2015, **161**, 1202–1214.

7 A. M. Klein, L. Mazutis, I. Akartuna, N. Tallapragada, A. Veres, V. Li, L. Peshkin, D. A. Weitz and M. W. Kirschner, *Cell*, 2015, **161**, 1187–1201.

8 F. Lan, B. Demaree, N. Ahmed and A. R. Abate, *Nat. Biotechnol.*, 2017, **35**, 640–646.

9 W. Zheng, S. Zhao, Y. Yin, H. Zhang, D. M. Needham, E. D. Evans, C. L. Dai, P. J. Lu, E. J. Alm and D. A. Weitz, *Science*, 2022, **376**, eabm1483.

10 K. Matuła, F. Rivello and W. T. S. Huck, *Adv. Biosyst.*, 2020, **4**, e1900188.

11 A. Stucki, J. Vallapurackal, T. R. Ward and P. S. Dittrich, *Angew. Chem., Int. Ed.*, 2021, **60**, 24368–24387.

12 F. Ma, M. T. Chung, Y. Yao, R. Nidetz, L. M. Lee, A. P. Liu, Y. Feng, K. Kurabayashi and G.-Y. Yang, *Nat. Commun.*, 2018, **9**, 1030.

13 F. Gielen, R. Hours, S. Emond, M. Fischlechner, U. Schell and F. Hollfelder, *Proc. Natl. Acad. Sci. U. S. A.*, 2016, **113**, E7383–E7389.

14 S. Sarkar, N. Cohen, P. Sabhachandani and T. Konry, *Lab Chip*, 2015, **15**, 4441–4450.

15 M. Courtney, X. Chen, S. Chan, T. Mohamed, P. P. N. Rao and C. L. Ren, *Anal. Chem.*, 2017, **89**, 910–915.

16 C. Holtze, A. C. Rowat, J. J. Agresti, J. B. Hutchison, F. E. Angilè, C. H. J. Schmitz, S. Köster, H. Duan, K. J. Humphry, R. A. Scanga, J. S. Johnson, D. Pisignano and D. A. Weitz, *Lab Chip*, 2008, **8**, 1632–1639.

17 H. Lee, C.-H. Choi, A. Abbaspourrad, C. Wesner, M. Caggioni, T. Zhu, S. Nawar and D. A. Weitz, *Adv. Mater.*, 2016, **28**, 8425–8430.

18 X. Li, S.-Y. Tang, Y. Zhang, J. Zhu, H. Forgham, C.-X. Zhao, C. Zhang, T. P. Davis and R. Qiao, *Angew. Chem., Int. Ed.*, 2024, **63**, e202315552.

19 L. Mazutis and A. D. Griffiths, *Lab Chip*, 2012, **12**, 1800–1806.

20 E. Brouzes, M. Medkova, N. Savenelli, D. Marran, M. Twardowski, J. B. Hutchison, J. M. Rothberg, D. R. Link, N. Perrimon and M. L. Samuels, *Proc. Natl. Acad. Sci. U. S. A.*, 2009, **106**, 14195–14200.

21 L. Mazutis, J.-C. Baret, P. Treacy, Y. Skhiri, A. F. Araghi, M. Ryckelynck, V. Taly and A. D. Griffiths, *Lab Chip*, 2009, **9**, 2902–2908.

22 A. Sciambi and A. R. Abate, *Lab Chip*, 2014, **14**, 2605–2609.

23 D. J. Eastburn, A. Sciambi and A. R. Abate, *Anal. Chem.*, 2013, **85**, 8016–8021.

24 A. R. Abate, T. Hung, P. Mary, J. J. Agresti and D. A. Weitz, *Proc. Natl. Acad. Sci. U. S. A.*, 2010, **107**, 19163–19166.

25 C. N. Baroud, M. R. de Saint Vincent and J.-P. Delville, *Lab Chip*, 2007, **7**, 1029–1033.

26 M. Sesen, A. Fakhfouri and A. Neild, *Anal. Chem.*, 2019, **91**, 7538–7545.

27 V. Bussiere, A. Vigne, A. Link, J. McGrath, A. Srivastav, J.-C. Baret and T. Franke, *Anal. Chem.*, 2019, **91**, 13978–13985.

28 R. Seemann, M. Brinkmann, T. Pfohl and S. Herminghaus, *Rep. Prog. Phys.*, 2011, **75**, 016601.

29 N. Bremond, A. R. Thiam and J. Bibette, *Phys. Rev. Lett.*, 2008, **100**, 024501.

30 L. Mazutis, J.-C. Bareta and A. D. Griffiths, *Lab Chip*, 2009, **9**, 2665–2672.

31 L. Mazutis and A. D. Griffiths, *Lab Chip*, 2012, **12**, 1800–1806.
32 T. M. Tran, F. Lan, C. S. Thompson and A. R. Abate, *J. Phys. D: Appl. Phys.*, 2013, **46**, 114004.
33 Y. Skhiri, P. Gruner, B. Semin, Q. Brosseau, D. Pekin, L. Mazutis, V. Goust, F. Kleinschmidt, A. E. Harrak, J. B. Hutchison, E. Mayot, J.-F. Bartolo, A. D. Griffiths, V. Taly and J.-C. Baret, *Soft Matter*, 2012, **8**, 10618–10627.
34 G. Etienne, A. Vian, M. Biočanin, B. Deplancke and E. Amstad, *Lab Chip*, 2018, **18**, 3903–3912.
35 P. Gruner, B. Riechers, B. Semin, J. Lim, A. Johnston, K. Short and J.-C. Baret, *Nat. Commun.*, 2016, **7**, 10392.
36 F. Courtois, L. F. Olguin, G. Whyte, A. B. Theberge, W. T. S. Huck, F. Hollfelder and C. Abell, *Anal. Chem.*, 2009, **81**, 3008–3016.
37 P. A. Sandoz, A. J. Chung, W. M. Weaver and D. Di Carlo, *Langmuir*, 2014, **30**, 6637–6643.
38 J. Cheng, J.-F. Chen, M. Zhao, Q. Luo, L.-X. Wen and K. D. Papadopoulos, *J. Colloid Interface Sci.*, 2007, **305**, 175–182.
39 T. Megyes, T. Grósz, T. Radnai, I. Bakó and G. Pálinkás, *J. Phys. Chem. A*, 2004, **108**, 7261–7271.
40 E. Owczarek and E. Hawlicka, *J. Phys. Chem. B*, 2006, **110**, 22712–22718.
41 K. Y. Lee and D. J. Mooney, *Prog. Polym. Sci.*, 2012, **37**, 106–126.
42 S. Maiti, K. Singha, S. Ray, P. Dey and B. Sa, *Pharm. Dev. Technol.*, 2009, **14**, 461–470.
43 E. A. Silva and D. J. Mooney, *Biomaterials*, 2010, **31**, 1235–1241.
44 P. Ghaderinejad, N. Najmoddin, Z. Bagher, M. Saeed, S. Karimi, S. Simorgh and M. Pezeshki-Modaress, *Chem. Eng. J.*, 2021, **420**, 130465.
45 J. Lee, J. Hong, W. Kim and G. H. Kim, *Carbohydr. Polym.*, 2020, **250**, 116914.
46 T. Liu, S. Yi, G. Liu, X. Hao, T. Du, J. Chen, T. Meng, P. Li and Y. Wang, *Carbohydr. Polym.*, 2021, **258**, 117702.
47 Y. Zhang, Y. Liu, C. Dong, R. Li, X. Zhang, T. Wang and K. Zhang, *Int. J. Biol. Macromol.*, 2024, **276**, 134107.
48 D. Indana, P. Agarwal, N. Bhutani and O. Chaudhuri, *Adv. Mater.*, 2021, **33**, 2101966.
49 M. H. Kim, D. Banerjee, N. Celik and I. T. Ozbolat, *Biofabrication*, 2022, **14**, 024103.
50 M. Chen, G. Bolognesi and G. T. Vladisavljević, *Molecules*, 2021, **26**, 3752.
51 H. Zhang, E. Tumarkin, R. M. A. Sullan, G. C. Walker and E. Kumacheva, *Macromol. Rapid Commun.*, 2007, **28**, 527–538.
52 H. Zhang, E. Tumarkin, R. Peerani, Z. Nie, R. M. A. Sullan, G. C. Walker and E. Kumacheva, *J. Am. Chem. Soc.*, 2006, **128**, 12205–12210.
53 C. Kim, J. Park and J. Y. Kang, *Biomicrofluidics*, 2014, **8**, 066504.
54 M. Lian, C. P. Collier, M. J. Doktycz and S. T. Retterer, *Biomicrofluidics*, 2012, **6**, 044108.
55 D.-H. Lee, W. Lee, E. Um and J.-K. Park, *Biomicrofluidics*, 2011, **5**, 034117.
56 M. Samandari, F. Alipanah, S. H. Javanmard and A. Sanati-Nezhad, *Sens. Actuators, B*, 2019, **291**, 418–425.
57 C. Kim, K. S. Lee, Y. E. Kim, K.-J. Lee, S. H. Lee, T. S. Kim and J. Y. Kang, *Lab Chip*, 2009, **9**, 1294–1297.
58 F. Chen, Y. Zhan, T. Geng, H. Lian, P. Xu and C. Lu, *Anal. Chem.*, 2011, **83**, 8816–8820.
59 S. Utech, R. Prodanovic, A. S. Mao, R. Ostafe, D. J. Mooney and D. A. Weitz, *Adv. Healthcare Mater.*, 2015, **4**, 1628–1633.
60 A. G. Håti, D. C. Bassett, J. M. Ribe, P. Sikorski, D. A. Weitz and B. T. Stokke, *Lab Chip*, 2016, **16**, 3718–3727.
61 H. Ahmed and B. T. Stokke, *Lab Chip*, 2021, **21**, 2232–2243.
62 Y. M. Efremov, A. I. Shpichka, S. L. Kotova and P. S. Timashev, *Soft Matter*, 2019, **15**, 5455–5463.
63 M. Glaubitz, N. Medvedev, D. Pussak, L. Hartmann, S. Schmidt, C. A. Helmd and M. Delcea, *Soft Matter*, 2014, **10**, 6732–6741.
64 Y. Wang, T. Cao, J. Ko, Y. Shen, W. Zong, K. Sheng, W. Cao, S. Sun, L. Cai, Y.-L. Zhou, X.-X. Zhang, C. Zong, R. Weissleder and D. Weitz, *Adv. Sci.*, 2020, **7**, 1903463.
65 H. H. Hooper, J. P. Baker, H. W. Blanch and J. M. Prausnitz, *Macromolecules*, 1990, **23**, 1096–1104.
66 D. Lee, H. Zhang and S. Ryu, in *Cellulose-Based Superabsorbent Hydrogels*, ed. I. H. Mondal, Springer Cham, 1st edn, 2018, ch. 27, pp. 865–884.
67 Q. Li, L. Ma, Z. Gao, J. Yin, P. Liu, H. Yang, L. Shen and H. Zhou, *ACS Appl. Mater. Interfaces*, 2022, **14**, 41695–41711.
68 Q. Zhang, P. Su, F. Zhao, H. Ren, C. He, Q. Wu, Z. Wang, J. Ma, X. Huang and Z. Wang, *ACS Biomater. Sci. Eng.*, 2024, **10**, 2235–2250.
69 M. Ghezzi, S. Pescina, C. Padula, P. Santi, E. Del Favero, L. Cantù and S. Nicoli, *J. Controlled Release*, 2021, **332**, 312–336.
70 Y. Chen, A. W. Gani and S. K. Y. Tang, *Lab Chip*, 2012, **12**, 5093–5103.